

Supplementary Material: Data-driven integration of hippocampal CA1 synaptic physiology in silico

András Ecker, Armando Romani, Sára Sáray, Szabolcs Káli, Michele Migliore, Joanne Falck, Sigrun Lange, Audrey Mercer, Alex M. Thomson, Eilif Muller, Michael W. Reimann, Srikanth Ramaswamy

Supplementary Methods

Single cell models

Detailed biophysical models of PCs and interneurons of the CA1 region from Migliore et al. (2018) were used in the present study. The models are publicly available on [ModelDB:244688](#) and as a "live paper" of the Human Brain Project's (HBP's) Brain Simulation Platform (BSP), where they can be interrogated in a web browser without installing anything locally. Along the excitatory PCs, they modeled 11 inhibitory interneurons.

The full list of the interneurons - and their mapping to the morphological-types (m-types) defined on hippocampome.org (Wheeler et al., 2015) are as follows: stratum lacunosum moleculare (SLM): perforant path-associated (PPA) cell - Perforant Path-Associated; stratum radiatum (SR): Schaffer collateral-associated (SCA) cell - Schaffer Collateral-Associated; stratum pyramidale (SP): axo-axonic (AA) cell - Axo-axonic, bistratified (BS) cell - Bistratified, CCK+ basket cell (BC) - Basket CCK+, Ivy cell - Ivy, PV+ BC - Basket; stratum oriens (SO): back-projection (BP) cell - Back-Projection, BS - Oriens-Bistratified, O-LM cell - O-LM, trilaminar (Tri) cell - Trilaminar (Supplementary Figure S1A). Electrical types (e-types), based on the Petilla convention (Ascoli et al., 2008) were assigned to traces recorded *in vitro* and modeled accordingly. All PCs were classified as continuous accommodating cells (cAC). Interneurons were classified as cAC, bursting accommodating cells (bAC) and continuous non-accommodating cells (cNAC). Combining m- and e-types yielded 16 morpho-electrical types (me-types) (Supplementary Figure S1C) (Markram et al., 2015; Migliore et al., 2018).

Channel kinetics were based on those used in many previously published papers on hippocampal neurons (Migliore et al., 1999, 2005; Ascoli et al., 2010; Morse et al., 2010), and validated against a number of experimental findings on CA1 pyramidal neurons. Cell models were equipped with the following active membrane properties: transient sodium current (Na); A, D, and M types and a delayed rectifier potassium currents (K_A , K_D , K_M , and K_{DR}); L, N, and T types of calcium currents (Ca_L , Ca_N and Ca_T); the nonspecific I_h ; and two types of calcium-dependent potassium currents (slow: K_{Cas} and voltage-dependent: K_{Ca}). A simple calcium extrusion mechanism, with a single exponential decay of 100 ms, was also included in all compartments containing calcium channels.

All models were constrained with active dendritic conductances but were optimized using only somatic features. While the somatic responses to various step-current injections were correct, the dendrites of the single-cell models turned out to be too excitable, namely, single synaptic inputs ($g_{syn} = 1$ nS) were leading to spikelets and somatic spikes. For this reason, single-cell models were slightly re-optimized. The amplitude of the back-propagating action potential (in the apical trunk, 150 and 250 μm from the soma) as a dendritic feature was added to the list of objectives for PCs. As for the interneurons, homogeneous dendritic sodium channel densities were replaced with one that decays exponentially with distance from the soma (with a length

constant of $50 \mu m$) based on Hu et al. (2010). A-type potassium channels in the dendrites of interneurons were also replaced with one that activates at a more hyperpolarized potential (see kinetics of "*kad*" for distal vs. "*kap*" for proximal A-type K^+ channels in Migliore et al. (1999)). Furthermore, the upper bounds (used by the multi-objective optimization algorithm) of dendritic sodium channel densities were reduced for all cell types. See re-optimized ion channel conductance in Supplementary Figure S1 B. After the re-optimization, single cells qualitatively reproduced the behavior presented in Migliore et al. (2018), assessed by *HippoUnit*, our single-cell model comparison framework.

The HippoUnit package contains standardized validations of biophysically detailed, multicompartmental single hippocampal PC models and is publicly available on Github under [/KaliLab/hippounit](#). Moreover, a demo validation of the re-optimized cell models was added as a use case in the BSP and is publicly available (again in a web browser without downloading and installing anything) upon registration to the HBP collaboratory.

Different versions of the Tsodyks-Markram model

The Tsodyks-Markram (TM) model of short-term plasticity (STP) underwent many changes in the last twenty years. For a recent and consistent review see Hennig (2013). Furthermore, the equations are sometimes shown in the form of differential equations (Tsodyks and Markram, 1997; Tsodyks et al., 2000; Fuhrmann et al., 2002, 2004; Loebel et al., 2009; Hennig, 2013), while in other papers the iterative solution evaluated at spike arrivals is presented (Markram et al., 1998; Maass and Markram, 2002). The version used in this article follows the formalism presented in Hennig (2013):

$$\begin{aligned}\frac{dR(t)}{dt} &= \frac{1 - R(t)}{D} - U(t)R(t)\delta(t - t_{spike}) \\ \frac{dU(t)}{dt} &= \frac{U_{SE} - U(t)}{F} + U_{SE}(1 - U(t))\delta(t - t_{spike})\end{aligned}$$

where $R(t)$ is the fraction of available resources, $U(t)$ is the release probability, D , and F are depression and facilitation time constants respectively. U_{SE} is the utilization of synaptic efficacy or absolute release probability (also known as the release probability in the absence of facilitation). $\delta(t)$ is the Dirac delta function and t_{spike} indicates the timing of a presynaptic spike. Each action potential in a train elicits an $A_{SE}U(t_{spike})R(t_{spike})$ amplitude PSC, where A_{SE} is the absolute synaptic efficacy and is linked to the Nq part of the quantal model, where N is the number of release sites and q is the quantal amplitude. $R = 1$, and $U = U_{SE}$ are assumed before the first spike. In our simulations, we implement Fuhrmann et al. (2002) as the stochastic generalization of the model. (Where the value of $U(t)$ is actually used as a *probability*.) The equation of the release probability is slightly different in that article and it reads as follows:

$$\frac{dU(t)}{dt} = -\frac{U(t)}{F} + U_{SE}(1 - U(t))\delta(t - t_{spike})$$

According to this equation $U(t)$ decays to 0 (the wording of the articles suggest a decay to "*the baseline*"). To recover the definition of U_{SE} as the release probability in absence of spikes (or U as the constant release probability in the first Tsodyks and Markram (1997) paper concentrating only on depressing connections) the $+U_{SE}(1 - U(t))$ has to be evaluated before the release happens. On the other hand, the $-U(t)R(t)$ jump in the equation of R still has to be evaluated after the event in order to be consistent with R being 1 in the absence of spikes. In this view $U(t)$ is mostly zero and at spike arrivals, before release happens it jumps to U_{SE} . From the biophysical point of view, this can be seen as a calcium-based model, where a quick calcium influx leads to release. On the other hand, in the Hennig (2013) version $U(t)$ decays to its baseline U_{SE} value and the $U_{SE}(1 - U(t))$ jump happens after the release. When fitting the deterministic TM model

to experimental data as well as when simulating the stochastic version we use an event-based solution, meaning that the equations are only evaluated at spike times (as opposed to the ODE form). For the Fuhrmann et al. (2002) version the iterative update is:

$$\begin{aligned} R_{tmp} &= 1 + (R_n - 1)\exp\left(-\frac{\Delta t}{D}\right) \\ U_{tmp} &= U_n \exp\left(-\frac{\Delta t}{F}\right) \\ U_{n+1} &= U_{tmp} + U_{SE}(1 - U_{tmp}) \\ A_{n+1} &= A_{SE}U_{n+1}R_{tmp} \\ R_{n+1} &= R_{tmp} - U_{n+1}R_{tmp} \end{aligned}$$

where Δt is the the time between the $(n + 1)$ th and n th spike and A_n is the n th amplitude. On the other hand, the Hennig (2013) version (used to fit models in Kohus et al. (2016)) is:

$$\begin{aligned} R_{tmp} &= 1 + (R_n - 1)\exp\left(-\frac{\Delta t}{D}\right) \\ U_{tmp} &= U_{SE} + (U_n - U_{SE})\exp\left(-\frac{\Delta t}{F}\right) \\ A_{n+1} &= A_{SE}U_{tmp}R_{tmp} \\ R_{n+1} &= R_{tmp} - U_{tmp}R_{tmp} \\ U_{n+1} &= U_{tmp} + U_{SE}(1 - U_{tmp}) \end{aligned}$$

None of these forms are presented in the literature per se. Both Markram et al. (1998) and Maass and Markram (2002) integrate the ODEs in a single step:

$$\begin{aligned} R_{n+1} &= 1 + (R_n - 1 - U_n R_n)\exp\left(-\frac{\Delta t}{D}\right) \\ U_{n+1} &= U_{SE} + (U_n - U_{SE} + U_{SE}(1 - U_n))\exp\left(-\frac{\Delta t}{F}\right) \\ &= U_{SE} + U_n(1 - U_{SE})\exp\left(-\frac{\Delta t}{F}\right) \\ &= U_n \exp\left(-\frac{\Delta t}{F}\right) + U_{SE}(1 - U_n \exp\left(-\frac{\Delta t}{F}\right)) \\ A_{n+1} &= A_{SE}U_{n+1}R_{n+1} \end{aligned}$$

Using the initialization $R_1 = 1$, $U_1 = U_{SE}$ and calculating the first two amplitudes with all 3 versions (Fuhrmann et al. (2002), Hennig (2013) and Maass and Markram (2002)) one gets:

$$\begin{aligned} A_1 &= A_{SE}U_{SE} \\ A_2 &= A_{SE}[U_{SE} + (U_{SE} - U_{SE}^2)\exp\left(-\frac{\Delta t}{F}\right)](1 - U_{SE}\exp\left(-\frac{\Delta t}{D}\right)) \end{aligned}$$

With simulations, it is also possible to show that all the other amplitudes in response to a spike train will be the same for all versions. Thus, the three event-based models presented above are equivalent. We present the Hennig (2013) formalism in the article since we find it more intuitive that both Dirac deltas are evaluated at the same point (after the PSC amplitude is calculated) and is more in line with the wording of the papers, but emphasize that it is consistent with the other version Fuhrmann et al. (2002) and the fits presented in Markram et al. (2015).

Membrane noise

In order to correctly compare the coefficient of variation (CV, std/mean) of first PSC amplitudes, measurement noise was added to the simulated traces (Barros-Zulaica et al., 2019). To this end, noise parameters of *in vitro* traces were fitted and averaged for every different connection types and then stochastic noise generated with these extracted parameters was added to the corresponding *in silico* traces. Noise was described as an Ornstein-Uhlenbeck (OU) process. The OU process is a stationary Gauss-Markov process, which describes the velocity of the movement of a Brownian particle and is used in physics to describe noise relaxation (Bibbona et al., 2008). Mathematically it can be described with the following iterative equation:

$$X(i) = X(i - 1) - \frac{X(i - 1)}{\tau}dt + \sigma\sqrt{\frac{2dt}{\tau}}\mathcal{N}(0, 1)$$

where dt is the time step of the signal, τ is the time constant fit to the exponential decay of the signal's autocorrelation function, σ is the standard deviation of the signal and $\mathcal{N}(0, 1)$ is a draw from the normal distribution.

Supplementary Figures

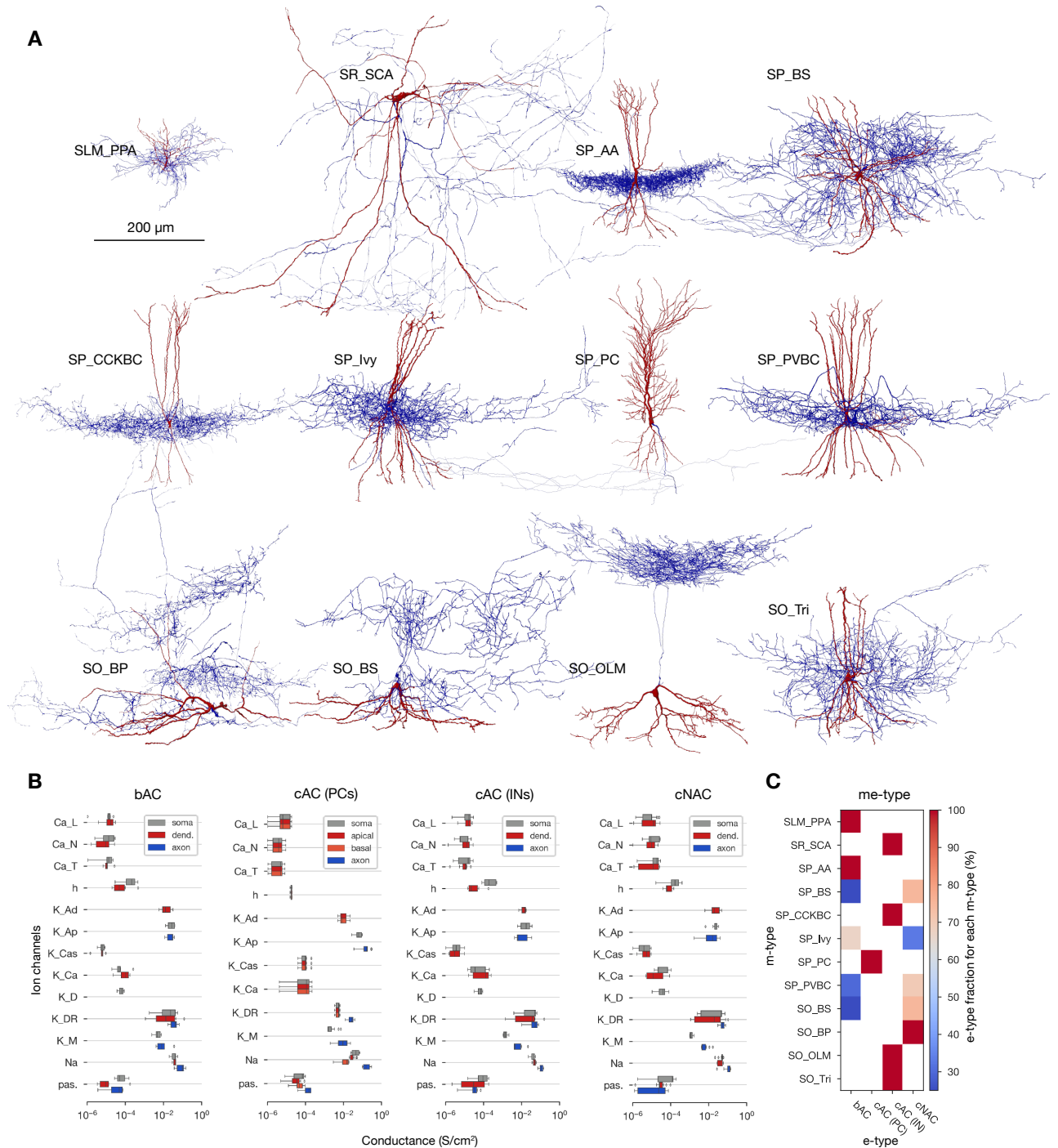


Figure S1: Single cell models. **A:** Exemplar 3D reconstructions of the 12 m-types in the CA1 network model. 3D morphologies were reconstructed with the NeuroLucida software by the members of the Thomson/Mercer lab (Migliore et al., 2018). Axons are shown in blue, while dendrites in red. Rendering and visualization was done with NeuroMorphoVis (Abdellah et al., 2018). Diameters are scaled ($\times 3$) for better resolution. **B:** Re-optimized ion channel conductances for all e-types (6 bAC, 13 cAC (PC), 7 cAC (IN) and 13 cNAC). Where non-uniform channel distribution was used (e.g. h current in PC dendrites) the maximal values are shown. **C:** Fraction of e-types (4) recorded and modeled in each of the 12 m-types.

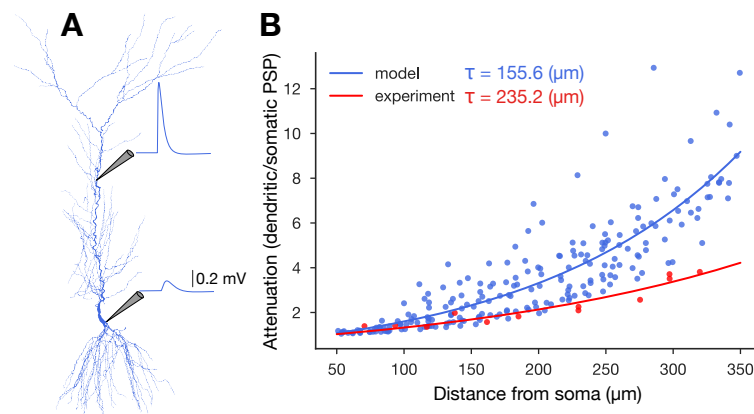


Figure S2: PSP attenuation. Validation of PSP attenuation against experimental data from Magee and Cook (2000). **A:** EPSC like currents were injected to the apical dendrites of the different pyramidal cell models from Migliore et al. (2018) and PSPs were measured at the injection site and at the soma. **B:** Summary of PSP attenuation (dendritic PSP/somatic PSP) in all PC models injected at different distances from the soma (in blue) and comparison to experimental data (in red).

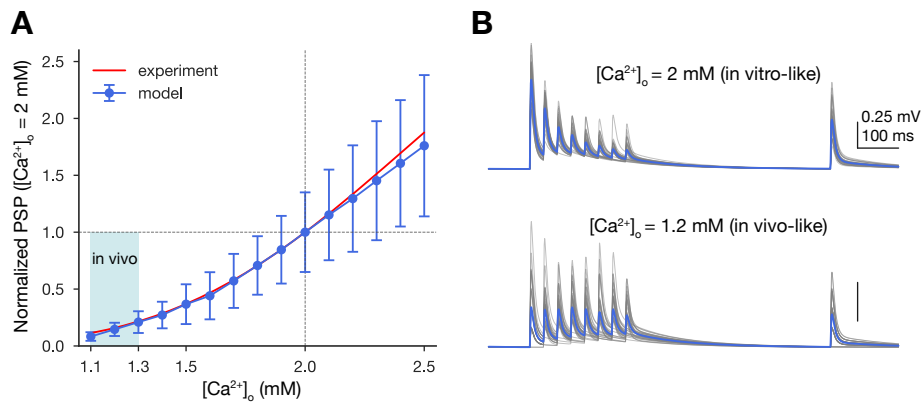


Figure S3: Calcium sensitivity of synaptic physiology. **A:** PC to PC PSP amplitudes at different extracellular calcium concentrations (normalized to 2 mM). Red curve indicates the experimentally measured scaling function which was applied to scale the U_{SE} parameter of the TM model. Shaded light blue area indicates the *in vivo* range 1.1-1.3 mM. **B:** Same *in silico* PC to PC pair at two different extracellular calcium concentrations. *In vitro* like is shown on top, while the *in vivo* one at the bottom. Single trials ($n = 35$) are shown in gray and their average in blue. Postsynaptic cells were held at -65 mV steady-state potential in *in silico* current-clamp mode. Vertical scale bar on the bottom panel represents the same value as the one on top.

Supplementary Tables

Table S1: Summary of paired recording experiments from rat CA1 in voltage-clamp mode (PSCs in pA). Liquid junction potentials (LJPs) and reversal potentials (E_{rev} s) are taken from Moradi and Ascoli (2019). Holding potentials (Hold.) are corrected for the indicated LJP with the correct sign. [†] in the rise time constant (τ_{rise}) column indicates 20-80% rise time, instead of 10-90%. PSC decay time constant (τ_{decay}) values are presented as in the original articles, without any normalization between fitting methods. Maccaferri et al. (2000) states that either single or weighted bi-exponential fit was applied, while the other sources do not determine the fitting method. M-type abbreviations are as in **Figure 3C**.

Presyn.	Postsyn.	Elect.	Ampl. (pA)	τ_{rise} (ms)	τ_{decay} (ms)	Hold. (mV)	[Ca ²⁺] (mM)	Temp. °C	E_{rev} (mV)	LJP (mV)	Reference
AA	PC	patch	308±103	0.8±0.1	11.2±0.9	-75.9	3	~30	-8.35	5.9	Maccaferri et al. (2000)
BS	PC	patch	Fig6) A,B	2±0.2	16.1±1.1	-75.9	3	~30	-8.35	5.9	Maccaferri et al. (2000)
CCKBC	PC	patch	118±13	0.73±0.05	6.8±0.2	-86.1	2	33	-95.1	16.1	Neu et al. (2007)
CCKBC	PC	patch	53.7±17.2	-	-	-86	2	33	-95.2	16	Földy et al. (2007)
CCKBC	PC	patch	23.6±8.25	2±0.8	9.35±1	-66.76	2.5	33±1	-94.45	16.76	Fuentealba et al. (2008)
CCKBC	PC	patch	115.4±10.8	0.63±0.04	6.47±0.27	-72.9±0.5	2	33	-90.3	14.6	Lee et al. (2010)
Ivy	PC	patch	8±2	2.8±0.2	16±2.5	-66.76	2.5	33±1	-94.45	16.76	Fuentealba et al. (2008)
OLM	PC	patch	26±10	6.2±0.6	20.8±1.7	-75.9	3	~30	-8.35	5.9	Maccaferri et al. (2000)
PVBC	PC	patch	43.6±17.9	-	-	-86	2	33	-95.2	16	Földy et al. (2007)
SCA	PC	patch	60.2±8.1	1.43±0.12	8.3±0.44	-72.7±0.8	2	33	-90.3	14.6	Lee et al. (2010)
OLM	PVBC	patch	11.7±1	2.6±1.3	16.5±3.9	-75.8	2	33±1	-112.2	15.8	Elfant et al. (2008)
OLM	SCA	patch	19.5±4.7	1.9±0.4	31.2±4.5	-75.8	2	33±1	-112.2	15.8	Elfant et al. (2008)

Table S2: Summary of paired recording experiments from rat CA1 in current-clamp mode (PSPs in mV). Liquid junction potentials (LJPs) and reversal potentials (E_{rev} s) are taken from Moradi and Ascoli (2019). Steady-state potentials (SSs) are corrected for the indicated LJP with the correct sign. † in the half width (HalfW.) column indicates PSP decay time constant instead of half width. M-type abbreviations are as in **Figure 3C**.

Presyn.	Postsyn.	Elect.	Ampl. (mV)	Rise (ms)	HalfW. (ms)	SS. (mV)	[Ca ²⁺] (mM)	Temp. °C	E_{rev} (mV)	LJP (mV)	Reference
PC	PC	sharp	0.7±0.5	2.7±0.19	16.8±4.1	-69.17–72.17	2.5	34-36	-8.5	-2.17	Deuchars and Thomson (1996)
AA	PC	sharp	0.51±0.07	5±0.2	45.6±2	-55.17±1	2.5	34-36	-73	-2.17	Pawelzik et al. (1999)
BS	PC	sharp	0.86±0.55	8.5±3.6	43.9±13.9	-59.77±4.4	2.5	34-36	-73	-2.17	Pawelzik et al. (1999)
BS	PC	sharp	0.55±0.15	7.4±1.4	54.6±4.2	-58.5±0.5	2.	34-36	-73	-0.6	Pawelzik et al. (2002)
BS	PC	sharp	0.8±0.6	8.4±3.2	42.1±17	-55.17±5.1	2.5	34-36	-73	-2.17	Fuentealba et al. (2008)
CCKBC	PC	sharp	1.17±0.44	5.4±2.5	35.5±19.5	-57.17–67.17	2.5	34-36	-73	-2.17	Ali et al. (1999)
CCKBC	PC	sharp	1.47±1.06	6±2.2	47.6±13.3	-57.17–62.17	2.5?	34-36	-73	-2.17	Thomson et al. (2000)
CCKBC	PC	sharp	0.7±0.5	6.5±1.5	44.2±10.1	-59.2±3.3	2.5	34-36	-73	-0.6	Pawelzik et al. (2002)
Ivy	PC	sharp	0.8±0.4	2.8±0.2	54.1±13.8	-59.17±2.6	2.5	34-36	-73	-2.17	Fuentealba et al. (2008)
PVBC	PC	sharp	0.45±0.24	4.6±3.2	32.4±18†	-60.95±4.6	2	34-35	-73	-3.36	Buhl et al. (1995)
PVBC	PC	sharp	1.17±0.57	4.5±2	30.4±11.6	-57.17–67.17	2.5	34-36	-73	-2.17	Ali et al. (1999)
PVBC	PC	sharp	0.81±0.92	6.8±2.7	47.2±16.9	-59.87±3.8	2.5	34-36	-73	-2.17	Pawelzik et al. (1999)
PVBC	PC	sharp	1.12±0.74	5.1±1.8	39.5±15.2	-57.17–62.17	2.5?	34-36	-73	-2.17	Thomson et al. (2000)
PVBC	PC	sharp	0.83±0.37	5.13±2.06	38.32±12	-59±3	2.5	34-36	-73	-0.6	Pawelzik et al. (2002)
SCA	PC	sharp	0.38	10±2.8	45±2.2	-59.1±0.5	2.5	34-36	-73	-0.6	Pawelzik et al. (2002)
Tri	PC	sharp	0.8	5.6	48.8	-59.1±0.5	2.5	34-36	-73	-0.6	Pawelzik et al. (2002)
PC	BS	sharp	3.4±3.1	1.2±0.5	7.6±2.6	-68.17	2.5	34-35	-8.5	-2.17	Ali et al. (1998)
PC	BS	sharp	0.95±0.3	1.2±0.2	10.4±1.6	-66.6±1	2.5	34-36	-8.5	-0.6	Pawelzik et al. (2002)
PC	BS	sharp	1.8±2.3	1.5±0.3	6.4±2.7	-71.67±5.7	2.5	34-36	-8.5	-2.17	Fuentealba et al. (2008)
PC	CCKBC	sharp	2±2.1	1±0.4	6.1±1.5	-67.6±3	2.5	34-36	-8.5	-0.6	Pawelzik et al. (2002)
PC	Ivy	sharp	2.9±2.2	1.5±0.3	11.5±1.5	-67.97±5.4	2.5	34-36	-8.5	-2.17	Fuentealba et al. (2008)
PC	OLM	sharp	0.93±1.06	1.2±0.5	7.5±0.7	-72.17±2.3	2.5	34-36	-8.5	-2.17	Ali and Thomson (1998)
PC	PVBC	sharp	1.4±1.05	0.88±0.44	5.4±2.2	-68.17	2.5	34-35	-8.5	-2.17	Ali et al. (1998)
PC	PVBC	sharp	3.51±2.9	1±0.3	5.74±1.78	-67.6	2.5	34-36	-8.5	-0.6	Pawelzik et al. (2002)
BC	BS	sharp	0.37	1	5.6	-58	2	34-35	-73	-3	Cobb et al. (1997)
BC	BS	sharp	1±0.4	1.65±0.5	15.6±2.8	-65.17±4.4	2.5	34-36	-73	-2.17	Pawelzik et al. (2003)
BC	BC	sharp	0.25	1.3	27	-62	2	34-35	-73	-3	Cobb et al. (1997)
BC	BC	sharp	1.1±0.47	2.5±0.9	18.7±9.1	-61.17±4	2.5	34-36	-73	-2.17	Pawelzik et al. (2003)
BS	BC	sharp	0.7±0.4	2.5±0.8	19.1±9.5	-61.87±2.7	2.5	34-36	-73	-2.17	Pawelzik et al. (2003)
SCA	SCA	sharp	0.5	5	34.3	-58.6	2.5	34-36	-73	-0.6	Pawelzik et al. (2002)
SCA	SCA	patch	0.6±0.41	7.0±1.38	41.1±12.5	-39.5	2	20-22	-79.5	15.5	Ali (2007)

Table S3: Validation of number of synapses per connections (see **Figure 3 B**). M-type abbreviations are as in **Figure 3 C**.

Presyn.	Postsyn.	Reference data	Model	Reference
PC	PC	1.2±0.4	1.26±0.6	Deuchars and Thomson (1996)
AA	PC	6.1	7±4.4	Buhl et al. (1994b)
BS	PC	6	6.5±3.2	Buhl et al. (1994a)
CCKBC	PC	8.3±0.8	8.6±3.9	Földy et al. (2010)
OLM	PC	10±7	11±5.2	Maccaferri et al. (2000)
PVBC	PC	11±0.6	11.3±5.4	Földy et al. (2010)
SCA	PC	5.3±1.2	5±1.8	Vida et al. (1998)
PC	OLM	2.8±0.8	2.8±1.2	Biro et al. (2005)
PVBC	PV+	1.54±1.08	2.6±1.3	Sik et al. (1995)
SCA	SCA	3.5±1.5	3±1.4	Ali (2011)

Table S4: Validation of the CV of first PSC amplitudes (see **Figure 4 B**). M-type abbreviations are as in **Figure 3 C**.

Presyn.	Postsyn.	Reference data	Model	Reference
AA	PC	0.29 ± 0.11	0.28 ± 0.13	Kohus et al. (2016)
CCKBC	PC	0.43 ± 0.14	0.36 ± 0.1	Kohus et al. (2016)
PVBC	PC	0.26 ± 0.06	0.28 ± 0.07	Kohus et al. (2016)
SCA	PC	0.38 ± 0.11	0.31 ± 0.08	Kohus et al. (2016)
CCKBC	CCKBC	0.18 ± 0.16	0.18 ± 0.1	Kohus et al. (2016)
PVBC	AA	0.45 ± 0.11	0.17 ± 0.09	Kohus et al. (2016)
PVBC	PVBC	0.17 ± 0.05	0.22 ± 0.02	Kohus et al. (2016)

Table S5: Validation of PSP amplitudes (see **Figure 4 C**). PC to CCKBC and Ivy are not shown on the figure for visualization purpose. In some cases (indicated with [†]) outliers were removed from the reference data (see published reference data in **Supplementary Table S2**). M-type abbreviations are as in **Figure 3 C**.

Presyn.	Postsyn.	Reference data (mV)	Model (mV)	Reference
PC	PC	0.7±0.5	0.68±0.43	Deuchars and Thomson (1996)
AA	PC	0.51±0.07	0.51±0.21	Pawelzik et al. (1999)
BS	PC	0.55±0.15	0.55±0.24	Pawelzik et al. (2002)
CCKBC	PC	0.7±0.5	0.68±0.26	Pawelzik et al. (2002)
Ivy	PC	0.8±0.4	0.82±0.35	Fuentealba et al. (2008)
PVBC	PC	0.83±0.37	0.83±0.23	Pawelzik et al. (2002)
SCA	PC	0.38	0.39±0.17	Pawelzik et al. (2002)
Tri	PC	0.8	0.81±0.36	Pawelzik et al. (2002)
PC	BS	0.95±0.3	0.96±0.54	Pawelzik et al. (2002)
PC	CCKBC	2±2.1	1.85±0.67	Pawelzik et al. (2002)
PC	Ivy	2.9±2.2	2.65±2	Fuentealba et al. (2008)
PC	OLM	0.3±0.13 [†]	0.3±0.21	Ali and Thomson (1998)
PC	PVBC	1±0.4 [†]	1±0.75	Ali et al. (1998)
(PV)BC	(PV)BC	0.25	0.25±0.15	Cobb et al. (1997)

References

- Abdellah, M., Hernando, J., Eilemann, S., Lapere, S., Antille, N., Markram, H., and Schürmann, F. (2018). NeuroMorphoVis: A collaborative framework for analysis and visualization of neuronal morphology skeletons reconstructed from microscopy stacks. *Bioinformatics*, 34(13):i574–i582.
- Ali, A. B. (2007). Presynaptic Inhibition of GABAA Receptor-Mediated Unitary IPSPs by Cannabinoid Receptors at Synapses Between CCK-Positive Interneurons in Rat Hippocampus. *Journal of Neurophysiology*, 98(2):861–869.
- Ali, A. B. (2011). CB1 modulation of temporally distinct synaptic facilitation among local circuit interneurons mediated by N-type calcium channels in CA1. *Journal of Physiology*, 105:1051–1062.
- Ali, A. B., Bannister, A. P., and Thomson, A. M. (1999). IPSPs elicited in CA1 pyramidal cells by putative basket cells in slices of adult rat hippocampus. *European Journal of Neuroscience*, 11(5):1741–1753.
- Ali, A. B., Deuchars, J., Pawelzik, H., and Thomson, A. M. (1998). CA1 pyramidal to basket and bistratified cell EPSPs: Dual intracellular recordings in rat hippocampal slices. *Journal of Physiology*, 507(1):201–217.
- Ali, A. B. and Thomson, A. M. (1998). Facilitating pyramid to horizontal oriens-alveus interneurone inputs: Dual intracellular recordings in slices of rat hippocampus. *Journal of Physiology*, 507(1):185–199.
- Ascoli, G. A. et al. (2008). Petilla terminology: Nomenclature of features of GABAergic interneurons of the cerebral cortex. *Nature Reviews Neuroscience*, 9(7):557–568.
- Ascoli, G. A., Gasparini, S., Medinilla, V., and Migliore, M. (2010). Local Control of Postinhibitory Rebound Spiking in CA1 Pyramidal Neuron Dendrites. *The Journal of neuroscience*, 30(18):6434–6442.
- Barros-Zulaica, N., Rahmon, J., Chindemi, G., Perin, R., Markram, H., Muller, E., and Ramaswamy, S. (2019). Estimating the Readily-Releasable Vesicle Pool Size at Synaptic Connections in a Neocortical Microcircuit. *Frontiers in Synaptic Neuroscience*, 11(29).
- Bibbona, E., Panfilo, G., and Tavella, P. (2008). The Ornstein–Uhlenbeck process as a model of a low pass filtered white noise. *Meteorologia*, 45(6):S117.
- Biro, A. A., Holderith, N. B., and Nusser, Z. (2005). Quantal Size Is Independent of the Release Probability at Hippocampal Excitatory Synapses. *Journal of Neuroscience*, 25(1):223–232.
- Buhl, E. H., Cobb, S. R., Halasy, K., and Somogyi, P. (1995). Properties of unitary IPSPs evoked by anatomically identified basket cells in the rat hippocampus. *European Journal of Neuroscience*, 7(9):1989–2004.
- Buhl, E. H., Halasy, K., and Somogyi, P. (1994a). Diverse sources of hippocampal unitary inhibitory postsynaptic potentials and the number of synaptic release sites. *Nature*, 368:823–828.
- Buhl, E. H., Han, Z.-S., Lörinczi, Z., Stezhka, V. V., Karnup, S. V., and Somogyi, P. (1994b). Physiological Properties of Anatomically Identified AxoAxonic in the Rat Hippocampus. *Journal of Neurophysiology*, 71(4):1289–1307.

- Cobb, S. R., Halasy, K., Vida, I., Nyíri, G., Tamás, G., Buhl, E. H., and Somogyi, P. (1997). Synaptic effects of identified interneurons innervating both interneurons and pyramidal cells in the rat hippocampus. *Neuroscience*, 79(3):629–648.
- Deuchars, J. and Thomson, A. M. (1996). CA1 pyramid-pyramid connections in rat hippocampus in vitro: Dual intracellular recordings with biocytin filling. *Neuroscience*, 74(4):1009–1018.
- Elfant, D., Pal, B. Z., Emptage, N., and Capogna, M. (2008). Specific inhibitory synapses shift the balance from feedforward to feedback inhibition of hippocampal CA1 pyramidal cells. *European Journal of Neuroscience*, 27(1):104–113.
- Földy, C., Lee, S.-h., Morgan, R. J., and Soltesz, I. (2010). Regulation of fast-spiking basket cell synapses by the chloride channel ClC-2. *Nature Neuroscience*, 13(9):1047–1049.
- Földy, C., Lee, S. Y., Szabadics, J., Neu, A., and Soltesz, I. (2007). Cell type – specific gating of perisomatic inhibition by cholecystokinin. *Nature neuroscience*, 10(9):1128–1130.
- Fuentealba, P., Begum, R., Capogna, M., Jinno, S., Márton, L. F., Csicsvari, J., Thomson, A., Somogyi, P., and Klausberger, T. (2008). Ivy Cells: A Population of Nitric-Oxide-Producing, Slow-Spiking GABAergic Neurons and Their Involvement in Hippocampal Network Activity. *Neuron*, 57(6):917–929.
- Fuhrmann, G., Cowan, A., Segev, I., Tsodyks, M., and Stricker, C. (2004). Multiple mechanisms govern the dynamics of depression at neocortical synapses of young rats. *Journal of Physiology*, 557(2):415–438.
- Fuhrmann, G., Segev, I., Markram, H., and Tsodyks, M. (2002). Coding of Temporal Information by Activity-Dependent Synapses. *Journal of Neurophysiology*, 87(1):140–148.
- Hennig, M. H. (2013). Theoretical models of synaptic short term plasticity. *Frontiers in Computational Neuroscience*, 7(45).
- Hu, H., Martina, M., and Jonas, P. (2010). Dendritic mechanisms underlying rapid synaptic activation of fast-spiking hippocampal interneurons. *Science*, 327(5961):52–58.
- Kohus, Z., Káli, S., Schlinghoff, D., Papp, O., Rovira-Esteban, L., Freund, T. F., Hájos, N., and Gulyás, A. I. (2016). Properties and dynamics of inhibitory synaptic communication within the CA3 microcircuits of pyramidal cells and interneurons expressing parvalbumin or cholecystokinin. *The Journal of physiology*, 594(13):3745–74.
- Lee, S.-H., Földy, C., and Soltesz, I. (2010). Distinct endocannabinoid control of GABA release at perisomatic and dendritic synapses in the hippocampus. *The Journal of neuroscience*, 30(23):7993–8000.
- Loebel, A., Silberberg, G., Helbig, D., Markram, H., Tsodyks, M., and Richardson, M. J. E. (2009). Multiquantal release underlies the distribution of synaptic efficacies in the neocortex. *Frontiers in Cellular Neuroscience*, 3(27).
- Maass, W. and Markram, H. (2002). Synapses as dynamic memory buffers. *Neural Networks*, 15(2):155–161.
- Maccaferri, G., Roberts, J. D. B., Szucs, P., Cottingham, C. A., and Somogyi, P. (2000). Cell surface domain specific postsynaptic currents evoked by identified GABAergic neurones in rat hippocampus in vitro. *Journal of Physiology*, 524(1):91–116.
- Magee, J. C. and Cook, E. P. (2000). Somatic EPSP amplitude is independent of synapse location in hippocampal pyramidal neurons. *Nature neuroscience*, 3(9):895–903.

- Markram, H., Wang, Y., and Tsodyks, M. (1998). Differential signaling via the same axon of neocortical pyramidal neurons. *PNAS*, 95(9):5323–8.
- Markram, M., Muller, E., Ramaswamy, S., and Reimann, M. W. (2015). Reconstruction and Simulation of Neocortical Microcircuitry. *Cell*, 163:456–492.
- Migliore, M., Ferrante, M., and Ascoli, G. A. (2005). Signal Propagation in oblique dendrites of CA1 pyramidal cells. *Journal of Neurophysiology*, 94(6):4145–4155.
- Migliore, M., Hoffman, D. A., Magee, J. C., and Johnston, D. (1999). Role of an A-Type K⁺ Conductance in the Back-Propagation of Action Potentials in the Dendrites of Hippocampal Pyramidal Neurons. *Journal of Computational Neuroscience*, 7:5–15.
- Migliore, R., Lupascu, C. A., Bologna, L. L., Romani, A., Courcol, J.-D., Antonel, S., Van Geit, W. A. H., Thomson, A. M., Mercer, A., Lange, S., Falck, J., Rössert, C. A., Shi, Y., Hagens, O., Pezzoli, M., Freund, T. F., Kali, S., Muller, E. B., Schürmann, F., Markram, H., and Migliore, M. (2018). The physiological variability of channel density in hippocampal CA1 pyramidal cells and interneurons explored using a unified data-driven modeling workflow. *PLoS Computational Biology*, 14(9):e1006423.
- Moradi, K. and Ascoli, G. A. (2019). A comprehensive knowledge base of synaptic electrophysiology in the rodent hippocampal formation. *Hippocampus*.
- Morse, T., Carnevale, N., Mutalik, P., Migliore, M., and Shepherd, G. (2010). Abnormal excitability of oblique dendrites implicated in early Alzheimer’s: a computational study. *Frontiers in Neural Circuits*, 4(16).
- Neu, A., Földy, C., and Soltesz, I. (2007). Postsynaptic origin of CB1-dependent tonic inhibition of GABA release at cholecystokinin-positive basket cell to pyramidal cell synapses in the CA1 region of the rat hippocampus. *The Journal of physiology*, 578(1):233–247.
- Pawelzik, H., Bannister, A. P., Deuchars, J., Ilia, M., and Thomson, A. M. (1999). Modulation of bistratified cell IPSPs and basket cell IPSPs by pentobarbitone sodium, diazepam and Zn²⁺: Dual recordings in slices of adult rat hippocampus. *European Journal of Neuroscience*, 11(10):3552–3564.
- Pawelzik, H., Hughes, D. I., and Thomson, A. M. (2002). Physiological and morphological diversity of immunocytochemically defined parvalbumin- and cholecystokinin-positive interneurons in CA1 of the adult rat hippocampus. *Journal of Comparative Neurology*, 443(4):346–367.
- Pawelzik, H., Hughes, D. I., and Thomson, A. M. (2003). Modulation of inhibitory autapses and synapses on rat CA1 interneurons by GABAA receptor ligands. *Journal of Physiology*, 546(3):701–716.
- Sik, A., Penttonen, M., Ylinen, A., and Buzsáki, G. (1995). Hippocampal CA1 Interneurons: An in vivo Intracellular Labeling Study. *Journal of Neuroscience*, 10(15):6651–6665.
- Thomson, A. M., Bannister, A. P., Hughes, D. I., and Pawelzik, H. (2000). Differential sensitivity to Zolpidem of IPSPs activated by morphologically identified CA1 interneurons in slices of rat hippocampus. *European Journal of Neuroscience*, 12(2):425–436.
- Tsodyks, M. and Markram, H. (1997). The neural code between neocortical pyramidal neurons depends on neurotransmitter release probability. *PNAS*, 94:719–723.
- Tsodyks, M., Uziel, A., and Markram, H. (2000). Synchrony generation in recurrent networks with frequency-dependent synapses. *The Journal of neuroscience*, 20(RC50).

- Vida, I., Halasy, K., Szinyei, C., Somogyi, P., and Buhl, E. H. (1998). Unitary IPSPs evoked by interneurons at the stratum radiatum — stratum lacunosum-moleculare border in the CA1. *Journal of Physiology*, 506(3):755–773.
- Wheeler, D. W., White, C. M., Rees, C. L., Komendantov, A. O., Hamilton, D. J., and Ascoli, G. A. (2015). Hippocampome.org: A knowledge base of neuron types in the rodent hippocampus. *eLife*, 4(e09960).